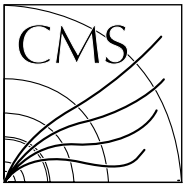

The Compact Muon Solenoid Experiment

CMS Note

Mailing address: CMS CERN, CH-1211 GENEVA 23, Switzerland

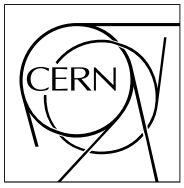

11 January 2001

Studies of the Global Muon Trigger Performance

H. Sakulin

CERN, Geneva, Switzerland

M. Fierro

Institute for High Energy Physics, Vienna, Austria

Abstract

The CMS L1 Global Muon Trigger combines the results of the three regional muon triggers to find the best four muon candidates in every bunch crossing. Its flexible hardware design consisting of Field Programmable Gate Arrays and memory-based Look-Up Tables allows the GMT algorithm to be adjusted for optimum performance according to the characteristics of the regional muon triggers.

The entire Level-1 trigger chain has been simulated with the object-oriented ORCA 4 simulation software. The presented study describes the performance of the regional Level-1 muon triggers and the optimization of the Global Muon Trigger algorithm using single muon and minimum bias samples. It is demonstrated that the GMT can achieve high efficiency in all regions of the detector, an extremely low number of ghosts and a trigger rate compatible with the projected L1 rates.

1 Introduction

The Compact Muon Solenoid (CMS) is one of two general purpose detectors at CERN's new Large Hadron Collider (LHC) which is planned to start operation in 2005. In the CMS detector large emphasis is given to the Muon System as it will allow identifying signatures of most of the physics channels investigated at LHC. The CMS Muon System [1] consists of three subsystems as illustrated in Figure 1: the Drift Tube (DT) System that covers the barrel region, the Cathode Strip Chamber (CSC) System that covers the two endcap regions and a Resistive Plate Chamber (RPC) System, which covers the whole detector and is specifically designed for trigger purposes. The DT chambers completely cover the region of pseudorapidity up to $|\eta| = 0.8$, the CSCs completely cover the pseudorapidity region of $1.2 < |\eta| < 2.4$, the region in between where muons pass through DT chambers and CSCs is called the overlap region.

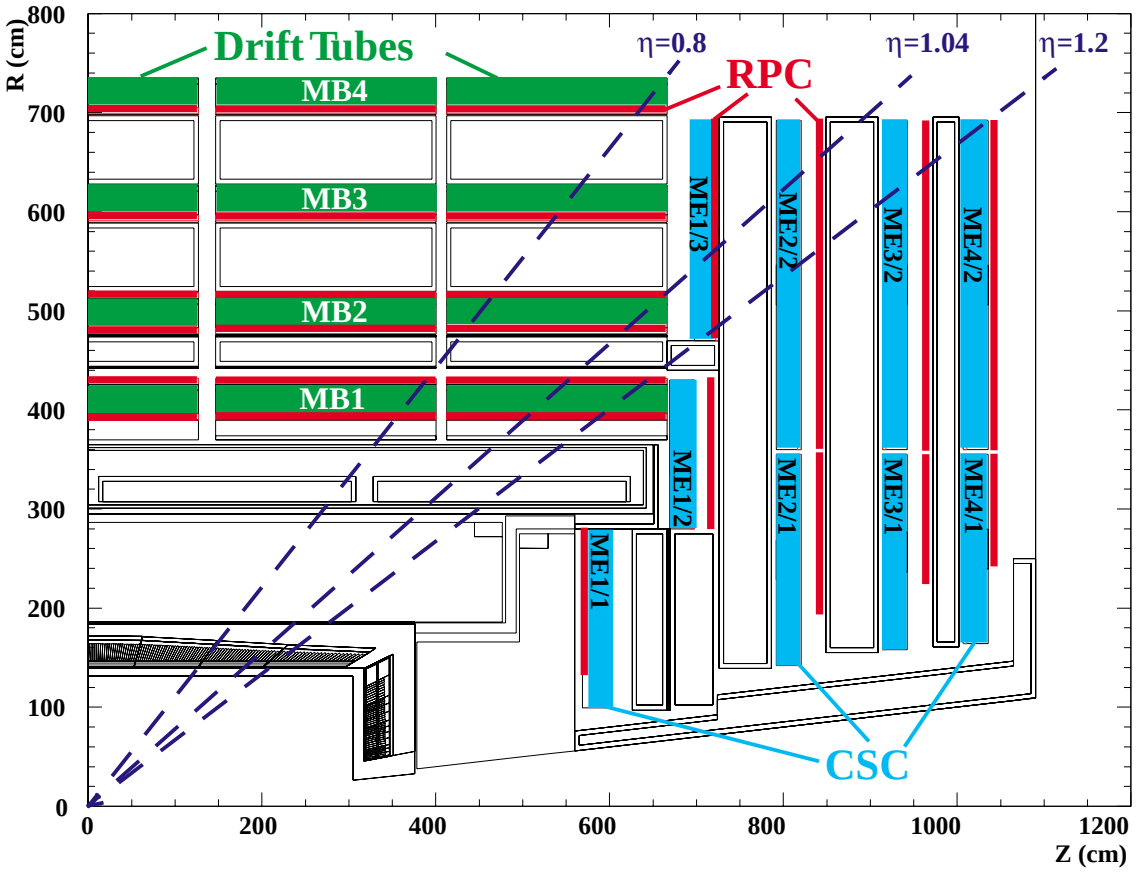

Figure 1: The CMS muon system, r-z-view

Due to the high luminosity of $10^{34}\,\mathrm{cm}^{-2}\mathrm{s}^{-1}$ the trigger system is of utmost importance. Its purpose is to reduce the data rate of 40 MHz (the LHC bunch crossing frequency) down to 100 Hz, which is the maximum rate that can be handled by the data acquisition system and the data storage system. The trigger system will be implemented in various stages (Levels). The Level-1 Trigger has to reduce the data rate from 40 MHz to 100 kHz, the maximum input rate of the High Level Triggers (HLT). It has to make its decision every 25 ns with a maximum delay of $3.2\,\mu$s or 128 bunch crossings (bx) including the time for signal propagation from the detector to the counting room and back. The entire L1 Trigger is therefore implemented in fully pipelined hardware.

All three muon systems participate in the Level-1 Trigger [2] of CMS as illustrated in Figure 2. The regional triggers of the DT, CSC and RPC system deliver lists of muon candidates found in their respective parts of the detector. The Global Muon Trigger (GMT) combines the muon candidates and finds the four highest-rank muon candidates of the whole detector in every bunch crossing. The ranks increase with p_T and quality of the muon candidate. The GMT exploits the complementarity of the muon systems in order to reach high efficiency and purity. It also attaches two bits from the Calorimeter Trigger to each muon data record, a Quiet bit indicating a calorimetric isolation condition and a Minimum Ionizing Particle (MIP) bit denoting compatibility with a minimum ionizing particle in the calorimeter system.

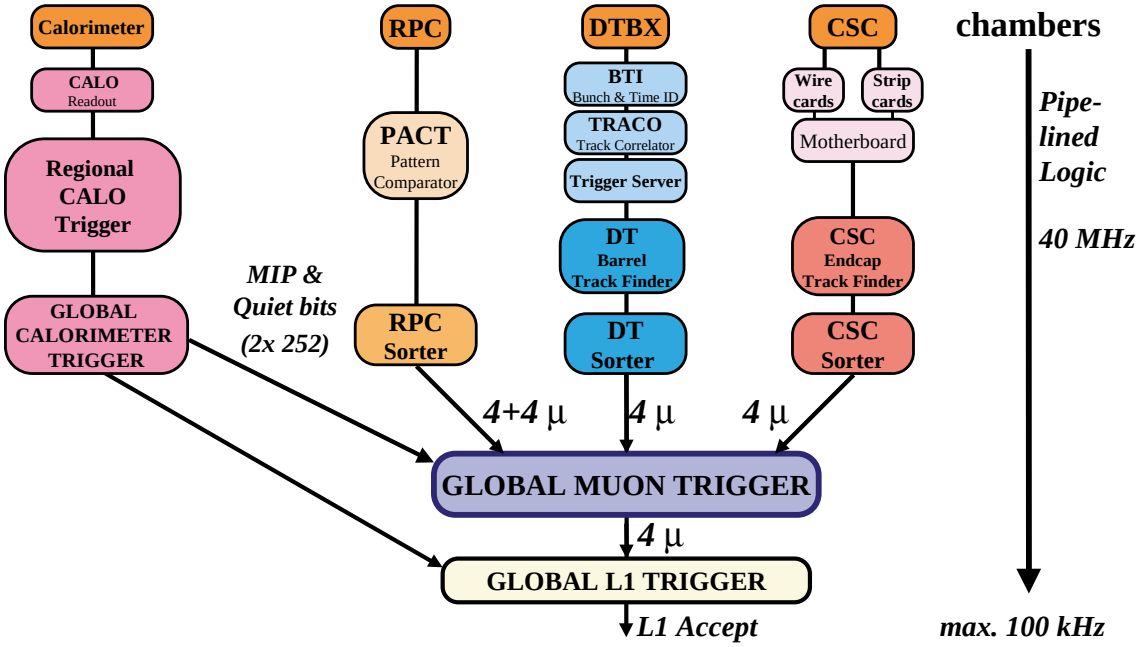

Figure 2: The CMS Level-1 Trigger

2 The Global Muon Trigger

The Global Muon Trigger is located in the Global Trigger Crate in the underground counting room. It receives its input data on cables from the neighboring regional muon trigger and calorimeter trigger crates and sends its output to the Global Trigger via the backplane. The detailed conceptual design of the GMT has been presented in Ref. [3]. Figure 3 illustrates the principle of the underlying algorithm. The GMT receives four input muon candidates from the DT trigger (barrel), four input muon candidates from the CSC trigger (endcaps) and eight candidates from the RPC trigger split into four from the barrel and four from the two endcaps. Each muon candidate is represented by a data word containing information about p_T (5 bits), ϕ (8 bits), η (6 bits), quality (3 bits) and charge (1 bit). The quality bits indicate the number of muon stations involved in the track and thereby the method used for p_T-assignment as detailed in Table 1.

One match logic compares the four DT muon candidates with the four barrel RPC muon candidates while a second one compares the four CSC muon candidates with the four forward RPC candidates. A match quality is calculated based on the proximity in space of the two candidates. A pair logic then determines the pairs with highest match quality and outputs a pair matrix that indicates for each pairing of muon candidates if they represent measurements of the same physical muon.

In parallel for each muon candidate a Single Rank is determined from the Single Rank Look-Up Tables (LUTs) based on their p_T, quality and pseudorapidity. The Single Rank is used for sorting if the muon candidate is unconfirmed. Otherwise, if the muon candidate is matched with a candidate from the complementary system, an increased rank is used for sorting. The Single Rank is also used in the Muon Merger Logic and in the Selection Logic.

The Muon Merger Logic uses the pair matrix and the Single Ranks to merge two measurements of the same physical muon. Different implementation options exist as discussed in Subsection 5.2.

The GMT Selection Logic decides whether a muon candidate detected by only one regional trigger will be forwarded or suppressed. This decision is based on the candidate's detector type, quality, p_T, and pseudorapidity as given by its Single Rank.

In parallel to the matching and merging procedure a projection logic extrapolates each muon candidate back to the calorimeter and attaches the MIP and a Quiet bits indicating compatibility with a minimum ionizing particle or an isolation condition.

Finally, the resulting muon candidates are sorted by their ranks in a two-stage sorter and the best four muon candidates of the whole detector are forwarded to the Global Trigger [4, 5]. The output muon candidates are represented by data words containing information about p_T (5 bits), ϕ (8 bits), η (6 bits), quality (3 bits), charge (1 bit), MIP (1bit) and Isolation (1bit).

Table 1: Quality bits set by the regional triggers. Note that the RPC trigger uses two different algorithms depending on the p_T of the muon. The high-p_T algorithm is based on one RPC plane in each muon station while the low-p_T algorithm is based on four RPC planes in the two inner muon stations in the barrel or 4 stations in the endcap with grouped strips.

Quality code	DTBX stations in track	CSC # of stations in track	RPC $p_T \geq 6$ GeV/c	RPC $p_T < 6$ GeV/c
7	1234	-	-	-
6	123, 124, 12-ME13	-	-	-
5	134	-	-	-
4	234	-	-	-
3	12, 13, 14, 1-ME13	≥ 3	4 stations	4 planes
2	23, 24, 2-ME13	2, one being ME1	3 stations, missing stn. 3 or 4	-
1	34	anything else	3 stations, missing stn. 1	-
0	no track	no track	3 stations, missing stn. 2	3 planes

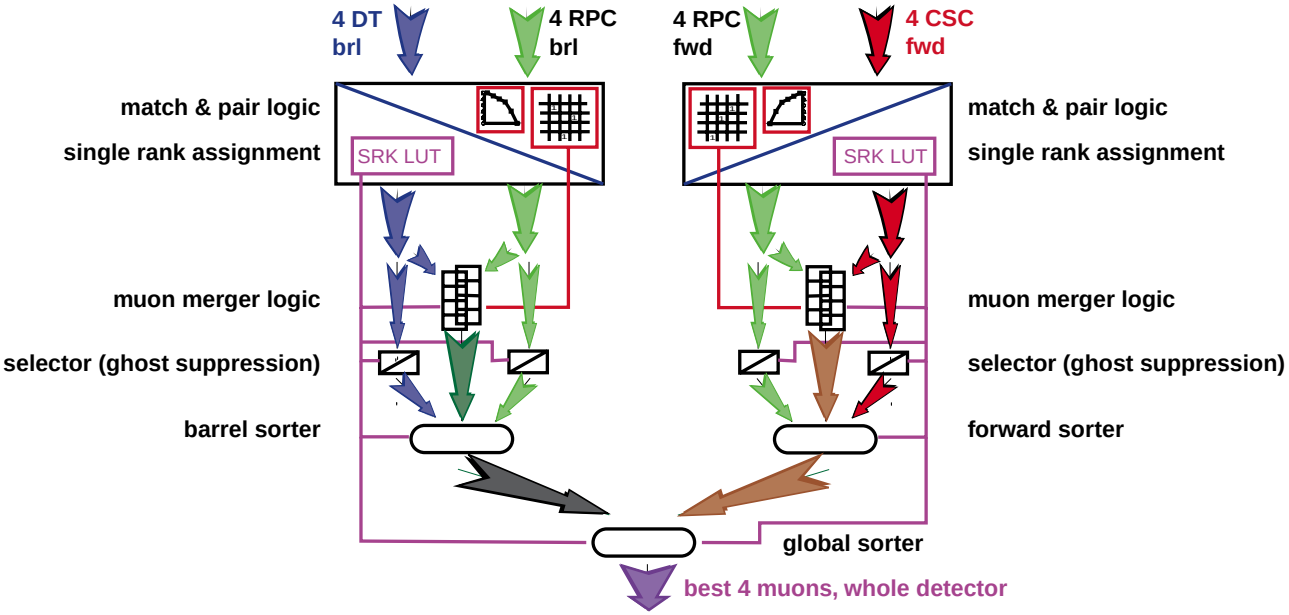

Figure 3: Principle of the CMS L1 Global Muon Trigger (Calorimeter projection logic not shown)

3 Simulation Software and Samples

Previous simulations of the GMT have been reported in Ref. [6]. For the present study, the detector has been simulated in CMSIM [7] version 118 (based on GEANT 3.21). The digitization, trigger primitive generation and simulation of the regional muon triggers and the Global Muon Trigger have been performed with the object-oriented simulation software package ORCA [8], version 4.3.2. An updated version of the CSC Track Finder simulation and an updated version of the Global Muon Trigger Simulation have been added.

For the simulation of efficiencies, ghosts, and turn-on-curves a sample of 100 000 single muon events has been used. The events are evenly distributed in charge, in η from -2.4 to 2.4, in ϕ from 0^o to 360^o and in p_T from 3 GeV/c to 100 GeV/c.

The background and trigger rate studies have been performed on the single muon minimum bias, W and Z samples described in Ref. [9]. Table 2 lists the utilized datasets. The events were generated with the PYTHIA 6.136 generator utilizing customized routines to force particles to decay into one muon and to correctly weight the events. Minimum bias samples with different cuts on the transverse momentum of the colliding partons ($\hat{p}_T$) and W and Z samples were added to increase statistics at high muon-p_T. In the digitization step an average of 17.3 events were piled up per bunch crossing corresponding to the total inelastic cross-section of 55 mb at the LHC design luminosity of L=10^{34} cm^{-2}s^{-1}.

Table 2: Generated Monte Carlo Data Sets for study of trigger rates.

Physics process	# of μ	$p_T^{\mu,min}$ (GeV/c)	# of events generated	# of events digitized	cross-section (mb)	int. luminosity (nb^{-1})
MB, $\hat{p}_T > 0$ GeV/c	1	1.5	2524437	160749	55.22	0.0448
MB, $\hat{p}_T > 5$ GeV/c	1	3.0	1234425	114496	25.65	0.0457
MB, $\hat{p}_T > 10$ GeV/c	1	4.0	1170638	135016	2.66	0.4405
MB, $\hat{p}_T > 20$ GeV/c	1	10.0	1146085	35405	0.26	4.3012
W + jets	1	3.0	584686	49000	1.85×10^{-4}	3161.9
Z/γ^* + jets	1	3.0	899205	49000	1.00×10^{-3}	898.0

4 Performance of the Regional Muon Triggers

4.1 Efficiencies and Ghosts

The DT/CSC and the RPC trigger systems show different efficiencies in η and ϕ and as a function of generated muon p_T due to geometry, construction properties and different trigger algorithms. Figure 4 shows the efficiencies of the regional muon triggers as a function of pseudorapidity. The efficiencies in Figures 4-8 are efficiencies to find exactly one muon of any measured p_T in an event in which one muon was generated. They include the geometric acceptance of the muon system as well as the chamber efficiencies. The DT system shows an efficiency above 95 % in regions covered by all four muon stations. The efficiency drops in the gaps between the barrel wheels, especially between wheel 0 and ± 1 around $|\eta| = 0.25$ and in the gap between barrel and endcap muon system around $|\eta| = 0.8$. Inclusion of endcap station ME1/3 into the barrel track finder recovers efficiency up to a pseudorapidity $|\eta| = 1.04$. In order to avoid finding the same muon in both the CSC and DT systems, a scheme [10] has been developed to ensure a sharp drop of the efficiency of the barrel track finder at $|\eta| = 1.04$ and a sharp rise of efficiency in the CSC track finder at the same point.

The CSC system shows an efficiency above 90 % up to $|\eta| = 2.4$ except around $|\eta| = 1.6$ and $|\eta| = 2.2$ where gaps between the rings of CSC chambers and partitioning of the strips inside the ME1/1 chambers cause inefficiencies. In the overlap region segments from barrel station MB1 are included in the CSC tracks. In order to maintain satisfactory p_T-resolution, CSC tracks are required to have a segment in station ME1 for $|\eta| > 1.2$, i.e. they have to be of quality codes 2 or 3. This explains the rather deep gap in efficiency around $|\eta| = 1.6$ and the slightly lower efficiency compared to the RPC system, overall. Note that the simulation of the CSC system assumes that station ME4 is present.

The RPC system shows high efficiency up to $|\eta| = 2.1$ except in the geometric cracks between the chambers. The shape and depth of the gaps in the efficiency is however quite different than in the DT and CSC system.

Figure 5 and Figure 6 show the efficiencies of the regional muon triggers as a function of the ϕ coordinate for the barrel ($|\eta| < 1.04$) and endcaps ($|\eta| > 1.04$), respectively. In the barrel the cracks between the chambers cause inefficiencies spaced at 30 ^{o} intervals. The efficiencies of DT and RPC show the same structure, the RPC efficiency showing slightly deeper drops in the geometrical cracks. This is because in the RPC system at least three out of four layers have to be hit to form a track while in the DT system also two-station tracks are allowed.

In the endcap the 10 ^{o} structure of the chambers is reflected in the track finding efficiency but due to the partly overlapping chambers it is less pronounced than in the barrel. Overall, the RPC efficiency is higher than the CSC efficiency in the endcap due to the requirements on CSC tracks mentioned above.

The efficiencies of the regional muon triggers and the GMT as a function of the transverse momentum of the generated muons are shown in Figure 7 and Figure 8 for the barrel and endcap, respectively. Above 5 GeV/c there is no dependence of the efficiencies on the p_T of the muons and all regional triggers reach a plateau above 90 % efficiency. For the barrel a sharp rise in efficiency at about 4 GeV/c can be seen.

Figure 9 shows the percentage of duplicated muons of any p_T (events in which one muon was generated and two were reported) in the regional muon triggers as a function of η. The DT track finder is largely free of ghosts, in the CSC track finder ghosts come mostly from the region of $|\eta| = 1.25$. The curve labeled "DTBX or CSC" shows the remaining percentage of muons seen by both the DT and by the CSC system in the overlap region after applying the scheme mentioned above. The RPC system shows a low rate of ghosts except in the region of $1.8 < |\eta| < 2.0$. The ghosts in this particular region are however reported with a very low p_T ($p_T < 3.5$ GeV/c) and are automatically suppressed if a p_T-cut is applied. Table 3 summarizes the overall efficiencies and percentages of ghosts for the three regional trigger subsystems.

Table 3: Efficiencies and Ghosts of the Regional Triggers and the GMT. Quoted efficiencies are efficiencies to find at least one muon of any p_T.

System	η coverage	Efficiency to find at least one muon	Percentage of Ghosts
RPC	$0 < \|\eta\| < 2.1$	94.4%	0.99%
DT	$0 < \|\eta\| < 1.04$	93.3%	0.10%
CSC	$1.04 < \|\eta\| < 2.4$	92.4%	0.34%

4.2 Turn-on Curves

Figures 10a-d show the turn-on curves as a function of the generated muon-p_T for several trigger thresholds. The measured p_T is defined at 90 % efficiency, i. e. a given measured p_T value indicates that there is a 90 % probability that the true p_T was less than or equal to the measured value. For the RPC system the turn-on curves are shown separately for barrel and endcap regions. The DT system reaches a plateau of about 93 % efficiency above the trigger threshold. The efficiency rises steeply just below the threshold reaching 90 % of the plateau efficiency at the trigger threshold. In the CSC system the plateau is slightly lower. The rise of efficiency is not as steep as in the barrel due to the lower resolution of the p_T-assignment in the endcap; the shape of the magnetic field in the endcap results in lower bending of the muons in ϕ and limits the achievable p_T resolution. The RPC system reaches a plateau of about 90 % efficiency in the barrel and about 93 % in the endcap. Due to the limited number of patterns at higher p_T, the RPC system tends to over-estimate the p_T so that the turn-on curves reach 90 % of the plateau efficiency already below the trigger threshold. Again, it can be seen that the p_T-resolution is lower in the endcap than in the barrel.

4.3 Trigger Rates

Figure 11 shows the integrated single muon trigger rates of the regional triggers as a function of the p_T threshold applied (defined at 90 % efficiency with the measured p_T being greater than or equal to the p_T cut) at a LHC luminosity of $10^{34}\,\mathrm{cm}^{-2}\mathrm{s}^{-1}$. The rates are based on the samples described in Section 3 using the full pile-up of an average of 17.3 events per bunch crossing. Two separate plots show the rates for DT and RPC in the barrel and CSC and RPC in the endcap. In these plots the generated muons as well as the reported muons have been restricted to the pseudorapidity ranges indicated in the plots. A combined plot shows the integrated single muon trigger rates for the whole detector. Each subsystem can be optimized to work in standalone mode and reduce the rate without confirmation of the complementary system. However, the best overall performance and robustness can only be achieved using the GMT. Therefore, the regional triggers do not apply any cuts on the reported muon candidates, which explains the high trigger rates of some of the regional triggers. In general, the trigger rates are lower than the rates of generated muons at a $p_T < 3\,\mathrm{GeV/c}$ since these muons do not reach the muon system and cannot be triggered. At high p_T the trigger rates are higher than the rates of generated muons due to noise and overestimation of the muon p_T by the trigger systems.

The maximum L1 trigger rate will be 100 kHz, initially however the High Level Triggers are planned for an input capacity of 75 kHz. This capacity may be adjusted through the purchase of additional computing nodes which can be rapidly installed. The uncertainties in estimates of cross sections at high energies and limited knowledge of branching ratios impose a large error on the estimated trigger rates. In addition we cannot assume that the CMS DAQ system will always run at its maximum design capacity. Therefore, we provide for a safety margin of a factor of three from the planned initial 75 kHz maximum L1 output rate to 25 kHz, in designing algorithms for L1 triggers. Furthermore, this 25 kHz bandwidth of L1 output has to be shared amongst both muon and calorimeter triggers. Therefore, we have selected a target rate of 12.5 kHz for the individual totals of the various calorimeter and muon triggers which leaves about 8-9 kHz for the single muon trigger. The trigger threshold for the single muon trigger is planned to be between 20 and 30 GeV/c at the LHC design luminosity of L=$10^{34}\,\mathrm{cm}^{-2}\mathrm{s}^{-1}$. At 25 GeV/c the trigger rates of the RPC and CSC systems are a factor of 3-5 higher than the available single muon trigger rate. In the next section it will be shown how the GMT can be optimized to reduce these trigger rates to sustainable levels.

5 Optimization of the GMT algorithm

Due to the use of FPGAs and memory-based LUTs the GMT is very flexible and its performance can be adjusted according to the performance of the regional muon triggers. Almost all adjustments can be done by loading new values into the LUTs. Only the adjustment of the Muon Merger Logic might require re-programming of the FPGA.

5.1 Optimization of the Muon Merger Logic

The Muon Merger Logic merges two measurements of the same physical muon. As stated above and detailed in Ref. [3] three implementation options exist for the Muon Merger Logic. These are

- the *winner/loser implementation*, which forwards all the parameters measured by one system and discards the parameters measured by the complementary system;
- the *parameter selection implementation*, which for each parameter selects the measurement of one system and discards the measurement of the complementary system;
- the *parameter mixing implementation*, which in addition to the above implementations combines the two measurements of a parameter using a LUT to obtain a new parameter.

The choice of Muon Merger Logic implementation has a significant impact on the p_T assignment and trigger rates. For this study the Muon Merger Logic has been simulated in winner/loser implementation and in parameter mixing implementation. In winner/loser implementation all the parameters of the muon candidate of higher rank are forwarded and the parameters of the matched candidate in the complementary system are discarded. The ranks are a function of quality and p_T and have been optimized for best p_T assignment. In parameter mixing implementation of the Muon Merger Logic the lower of the two measurements of the p_T is assigned to the output muon. The remaining parameters (η, ϕ, charge) are taken from the candidate with higher rank.

Figure 11d shows the effect of the Muon Merger Logic on the trigger rates. Assigning the lower p_T measurement reduces the trigger rates dramatically. For $p_T \geq 25\,\text{GeV/c}$ the rates are reduced by more than a factor of three compared to the rates with winner/loser implementation. Taking the lower of two measurements for the p_T is justified by the fact that the p_T measurement of the regional triggers indicates that a muon with a p_T "as large as" the measured value was detected. Using the 90% definition of the p_T scale there is theoretically only a 10% probability that the true p_T of the muon was larger than the measured value. In practice due to the limited resolution of the p_T scale the probability to overestimate the p_T of the muon is even larger than 90 %. *The parameter mixing implementation using the lower p_T measurement of the two systems is therefore adopted as default option for the Muon Merger Logic.*

5.2 Optimization of the Selection Logic

The Selection Logic decides whether a muon candidate that was detected by only one system will be forwarded or suppressed. This decision is made based on the candidate's quality, p_T, and η. The two extremes for the GMT selection would be a logical AND-algorithm that only takes muons seen by two systems and a logical OR-algorithm that accepts all muons even if they are seen by only one system. An AND-algorithm results in a very low number of ghosts and lowest possible trigger rates. The efficiency, however, will show deep gaps in some regions of ϕ and pseudorapidity. An OR-algorithm results in highest possible efficiency but it causes a high number of ghosts and too high trigger rates. An optimized algorithm can be obtained by making use of the quality information associated with each muon candidate (see Table 1). Muon candidates seen by two systems are accepted while muon candidates seen by only one system have to pass certain quality criteria. By this means a rather high efficiency, a low percentage of ghosts and acceptable trigger rates can be achieved.

The quality criteria depend on the detector type and region of pseudorapidity and have to be carefully tuned according to the performance of the regional triggers. The GMT Selection Logic has been optimized according to the simulated performance of the regional triggers resulting in a certain set of quality criteria. Thus the following types of muon candidates are rejected if they are unconfirmed:

RPC of quality code 1 in all RPC trigger towers ($0 < |\eta| < 2.1$): As can be seen from Figures 12c+d and Figures 13c+d, unmatched RPC muon candidates of quality code 1 contribute to the trigger rate before optimization, considerably, while contributing little to the overall efficiency.

RPC of quality code 0 in RPC trigger towers 5, 8-10, 14-16 ($0.7 < |\eta| < 0.83$**,** $1.04 < |\eta| < 1.36$ **and** $|\eta| > 1.73$**):** Figure 13c shows the regions where unmatched RPC muon candidates of quality code 0 contribute to the trigger rate. Also all the RPC ghosts shown in Figure 9 are of quality code 0. In towers 5 and 8-10 unmatched RPC muon candidates of quality 0 are suppressed to reduce the trigger rates, in towers 14-16 and also 8-10 they are suppressed to reduce ghosts. This type of muon candidates is kept in the other towers to avoid gaps in efficiency.

CSC of quality 2 or lower with $|\eta| \leq 2.1$**:** Figure 13b+d show the large contribution of unmatched CSC muon candidates of quality code 1 and 2 to the GMT trigger rates before optimization. Figure 12b+d show that they contribute comparably little to the efficiency below $|\eta| = 2.1$. As the region above $|\eta| = 2.1$ is only covered by the CSC system, the GMT cannot improve efficiency or rate. All quality codes of CSC candidates are accepted in this region.

CSC of any quality with $|\eta| < 1.06$ **and DT of any quality with** $|\eta| > 0.91$**:** In the overlap region muons can be found by both the DT and the CSC track finders even after applying a scheme to reduce the duplication at regional trigger level (see the curve labelled "DTBX+CSC" in Figure 9). As the RPC system does not show this problem the duplication can be avoided at the cost of some efficiency by requiring a confirmation by the RPC system. Unmatched DT and CSC muon candidates in the range $0.91 < |\eta| < 1.06$ are therefore suppressed.

6 Performance of the optimized GMT algorithm

6.1 Efficiencies and Ghosts

The efficiency of the optimized GMT as a function of η is shown in Figure 4. In most regions it is higher than the efficiency of the regional triggers, especially in the geometrical gaps between muon stations. Figure 14 compares the optimized GMT efficiency with the efficiency of an AND-algorithm and an OR-algorithm. Except for the overlap region, where some efficiency is traded for lower ghost rate, the efficiency of the optimized algorithm is very close to the high efficiency of the OR-algorithm.

Figures 5 and 6 show the efficiency of the Global Muon Trigger and as a function of the ϕ coordinate for the barrel ($|\eta| < 1.04$) and endcaps ($|\eta| > 1.04$), respectively. The GMT improves efficiency with respect to the regional muon triggers over the whole range.

The efficiency as a function of the transverse momentum of the generated muons is shown in Figure 7 and Figure 8 for the barrel and endcap, respectively. The GMT improves efficiency over the whole range.

Figure 9 shows the percentage of duplicated muons of any p_T (events in which one muon was generated and two were reported) as a function of η_{gen}. It is very important to control the ghosts as they can cause fake di-muon triggers. The physical rate of events with two muons is of the order of 1 % of the rate of single muon events. To prevent the di-muon trigger rates from being dominated by fakes, we demand that the ghosts are restricted to less than 0.5 % of the single muon events. The optimized Selection Logic of the GMT reduces the ghosts in all regions of pseudorapidity so that the overall ghost rate can be reduced to 0.18 %. Especially in the overlap region there are almost no remaining ghosts after requiring confirmation of DT and CSC candidates by the RPC system.

6.2 Turn-On Curves

Figures 10e+f show the turn-on curves for the GMT as a function of the generated muon p_T for several trigger thresholds (defined at 90 % efficiency) for the barrel and endcap regions, respectively. The GMT results in steeper turn-on curves than achievable with the respective regional muon triggers, which reach 90 % of the plateau efficiency at the trigger threshold.

6.3 Trigger Rates

Figures 11a-d show the integrated single muon trigger rates of the regional triggers and the GMT as a function of the p_T threshold applied (defined at 90 % efficiency with the measured p_T being greater than or equal to the p_T cut) at a LHC luminosity of $10^{34}\,\mathrm{cm}^{-2}\mathrm{s}^{-1}$.

Figures 11a-c show the situation in the barrel, endcap and whole detector, respectively. For the GMT the trigger rates are shown resulting from the fully optimized algorithm (curves labeled "GMT-opt") and from an AND-algorithm and an OR-algorithm using the Muon Merger Logic in parameter mixing implementation taking the

lower of the two p_T measurements in all cases. With the optimized GMT algorithm a trigger rate of 8.1 kHz, well inside the desired range, is reached for the whole detector at a trigger threshold of 25 GeV/c. For trigger thresholds between 10 and 60 GeV/c the trigger rate decreases sufficiently to control rates higher than expected. A big difference can be seen between the rates resulting from the AND- and OR-algorithms. The optimized algorithm reaches trigger rates almost as low as the AND-algorithm.

Figure 11d shows the effect of the Muon Merger Logic on the trigger rates. Using the parameter mixing implementation as described in Subsection 5.1 instead of the winner/loser implementation reduces the trigger rate at 25 GeV/c from 26.1 kHz to 8.1 kHz using the optimized GMT Selection Logic in both cases. The choice of the selection algorithm has much larger effect on the rates in parameter mixing implementation of the Muon Merger Logic than in winner/loser implementation since in the latter case the matched muon candidates dominate the rates. Table 4 summarizes the performance of the optimized GMT selection algorithm and compares it to the logical AND-algorithm and the logical OR-algorithm.

Table 4: Comparison of GMT performance with three different selection algorithms: optimized, logical OR and logical AND, using the Muon Merger Logic in parameter mixing implementation taking the lower of the two p_T-measurements in all cases. The performance with the optimized Selection Logic is the fully optimized performance found in this study.

GMT Algorithm	Efficiency	Ghosts	Trigger Rate $p_T > 25$ GeV/c
Logical OR	97.61%	1.60%	22.6 kHz
Logical AND	89.70%	0.07%	7.2 kHz
Optimized	*96.08%*	*0.18%*	*8.1 kHz*

6.4 Contributions to the Trigger Rates

Figure 15 shows the spectra of generated muons contributing to the L1 single muon trigger rates for various trigger thresholds. Due to the limited p_T resolution at Level-1 a large part of the trigger rates is caused by overestimating the p_T of low-p_T muons. In the barrel the spectra of contributing muons have a maximum slightly below the trigger threshold.

Figures 16a-c show the trigger rates caused by prompt muons and non-prompt muons (from π, K). The rates of generated prompt and non-prompt muons are shown in Figure 16d. Non-prompt low-p_T muons that result from decays outside the vertex can potentially be falsely recognized as high-p_T muons by the L1 trigger as they can cause segments similar to straight tracks coming from the vertex. It can be seen that this effect does not cause a large increase in the trigger rates.

7 Conclusion

A simulation study of the L1 muon trigger has been presented. The performance of the regional triggers of the DT, CSC and RPC system has been analyzed and the GMT algorithm has been optimized accordingly. It has been demonstrated that the GMT increases efficiency, greatly reduces ghosts and reduces the trigger rates so that the projected Level-1 trigger rates can be reached. The detailed settings obtained by the optimization are not intended to be final. They can be changed in hardware by changing the content of LUTs and they will change as the simulation models of the regional triggers evolve and finally when the actual performance of the regional triggers is known. The study demonstrates that the design of the GMT is flexible enough to accommodate changes in the performance of the regional triggers and still reach optimum performance.

Acknowledgements

The authors would like to thank Norbert Neumeister who converted the FORTRAN simulation of the GMT into C++ for use in the ORCA framework and cross-checked the L1 simulation results while working on the L2 trigger. Thanks have to be extended to the CMS High Level Trigger Group for providing the minimum bias samples used for the calculation of trigger rates. We are grateful to Grzegorz Wrochna for his numerous comments on the optimization of the Selection Logic and Muon Merger Logic. Last but not least the authors would like to thank Anton Taurok for the productive collaboration on all questions of hardware implementation of the GMT.

References

[1] **CERN/LHCC 1997-32** *"CMS, The Muon Project, Technical Design Report"* .

[2] **CERN/LHCC 2000-38**, *"CMS, The TriDAS Project, Technical Design Report, Volume 1: The Trigger Systems"*.

[3] **CMS Note, in preparation**, M. Fierro, N. Neumeister, P. Porth, H. Rohringer, H. Sakulin, A. Taurok, C.-E. Wulz, *"Conceptual Design of the First Level Global Muon Trigger for the CMS Experiment at LHC"*.

[4] **CMS Note 2000/052**, C.-E. Wulz, *"Concept of the First Level Global Trigger for the CMS Experiment at LHC"*.

[5] **CMS Note 2000/057**, A. Taurok, H. Bergauer, M. Padrta, *"Implementation and Synchronisation of the First Level Global Trigger for the CMS Experiment at LHC"*.

[6] **CMS Internal Note 1997/023**, N. Neumeister, P. Porth, H. Rohringer, *"Simulation of the Global Muon Trigger"*.

[7] CMS Simulation Package CMSIM, Users' Guide and Reference Manual, http://cmsdoc.cern.ch/cmsim/cmsim.html

[8] **CMS Internal Note 1999/035**, *"CMS Reconstruction Software, The ORCA Project"*.

[9] **CMS Internal Note 2000/053**, N. Neumeister, U. Gasparini, S. Lacaprara, A. Fanfani, H. Rick, A. Vitelli, *"Monte Carlo Simulation for High Level Trigger Studies in Single and Di-Muon Topologies"*.

[10] **CMS Internal Note, in preparation**, D. Acosta et al, *"Coverage of the DT/CSC Overlap Region by the Level-1 Track-Finders"*.

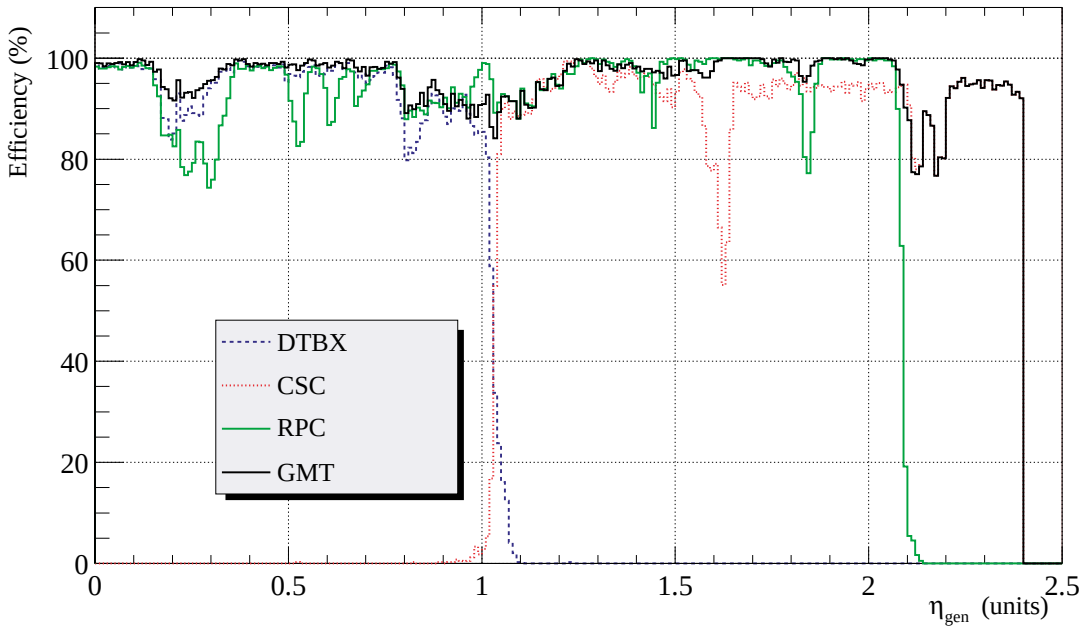

Figure 4: Efficiencies to find exactly one muon of any measured p_T for CSC, DT, RPC and GMT as a function of generated η. GMT fully optimized as described in Section 5.

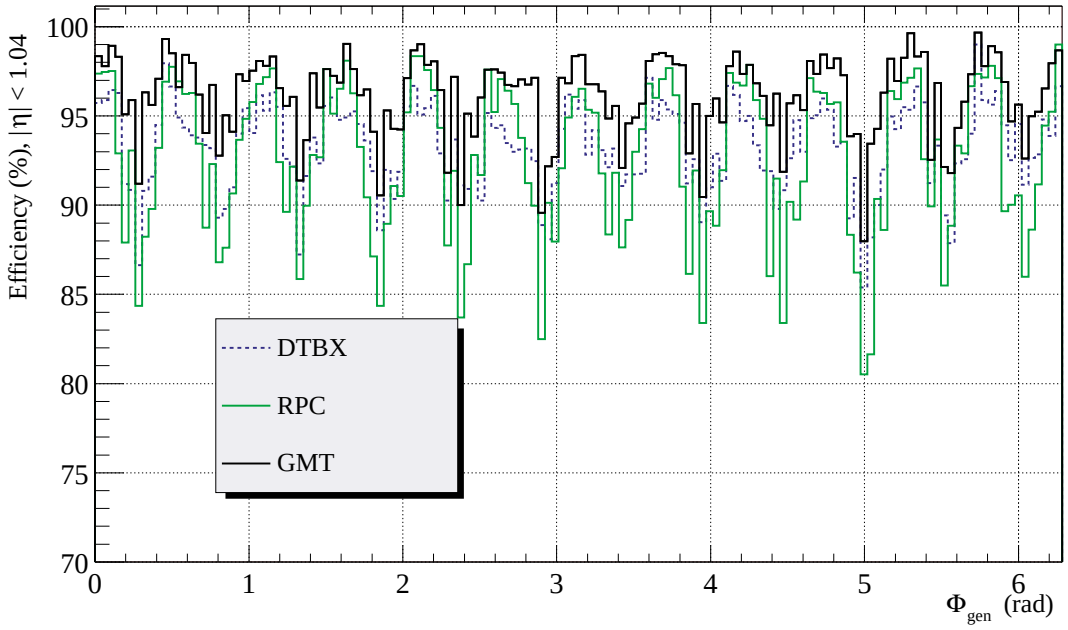

Figure 5: Efficiencies to find exactly one muon of any measured p_T for CSC, DT, RPC and GMT as a function of generated ϕ, barrel. GMT fully optimized as described in Section 5.

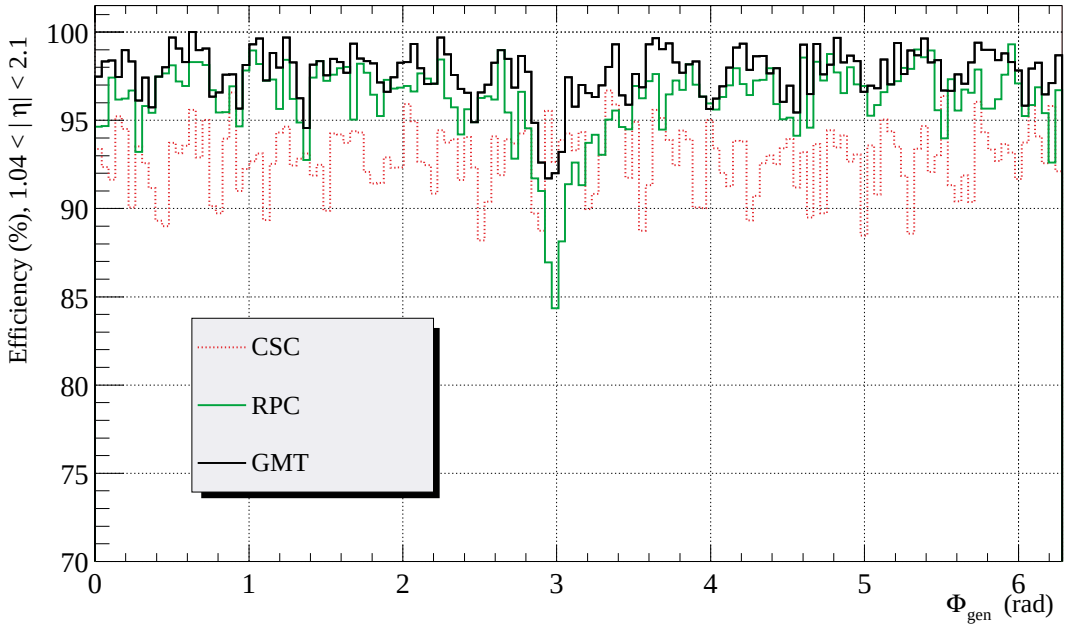

Figure 6: Efficiencies to find exactly one muon of any measured p_T for CSC, DT, RPC and GMT as a function of generated ϕ, endcaps. GMT fully optimized as described in Section 5. The drop in efficiency around $\phi = 3$ rad is caused by an artefact of the RPC geometry simulation which has been corrected in a subsequent version.

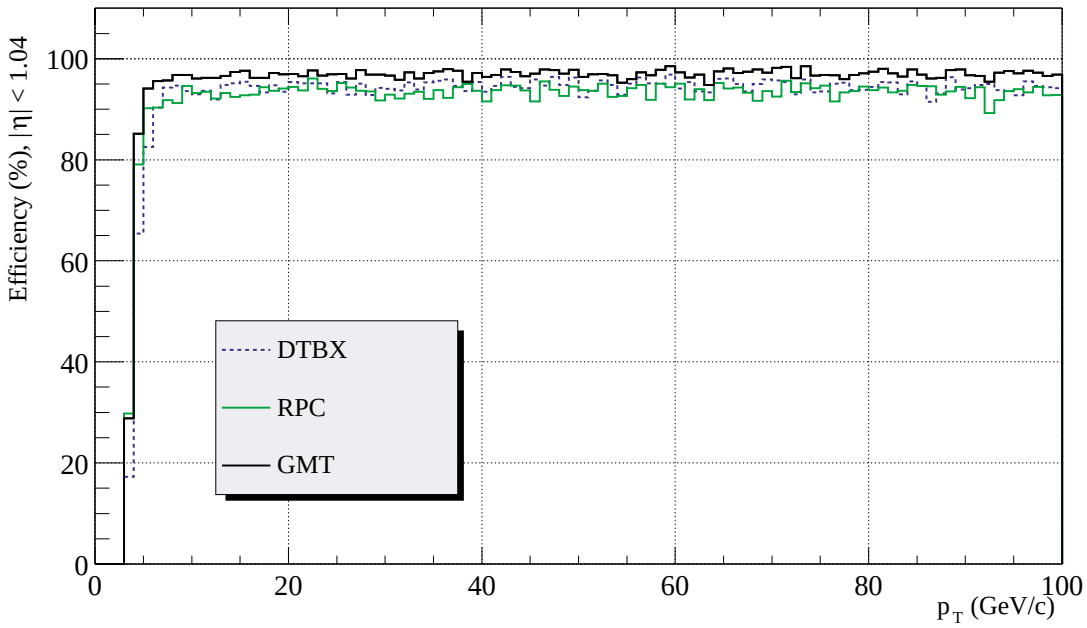

Figure 7: Efficiencies to find exactly one muon of any measured p_T for CSC, DT, RPC and GMT as a function of generated p_T, barrel. GMT fully optimized as described in Section 5.

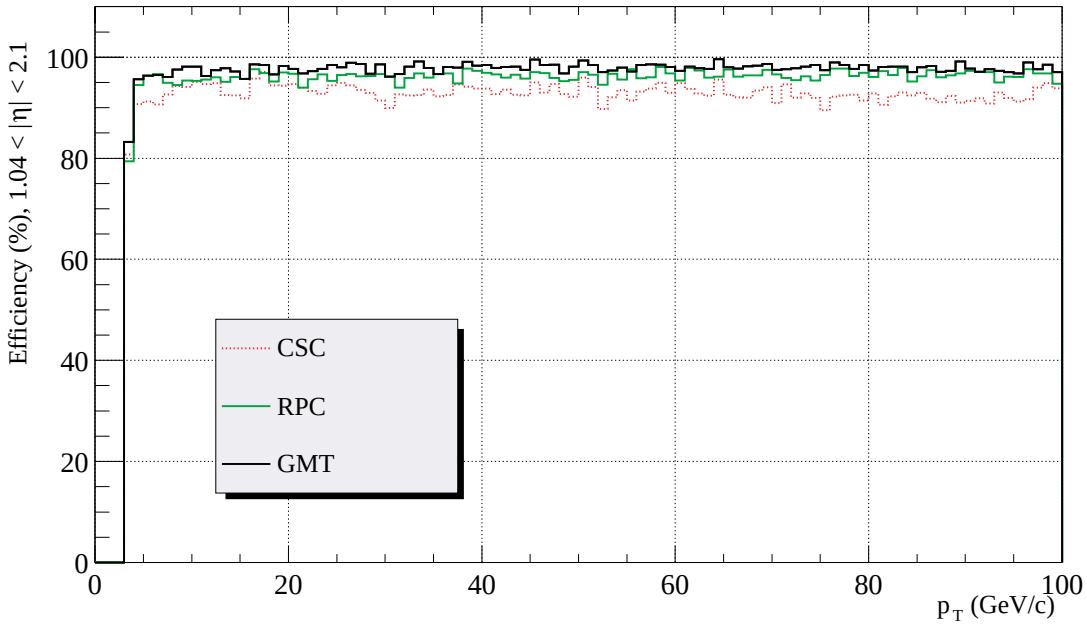

Figure 8: Efficiencies to find exactly one muon of any measured p_T for CSC, DT, RPC and GMT as a function of generated p_T, endcaps. GMT fully optimized as described in Section 5.

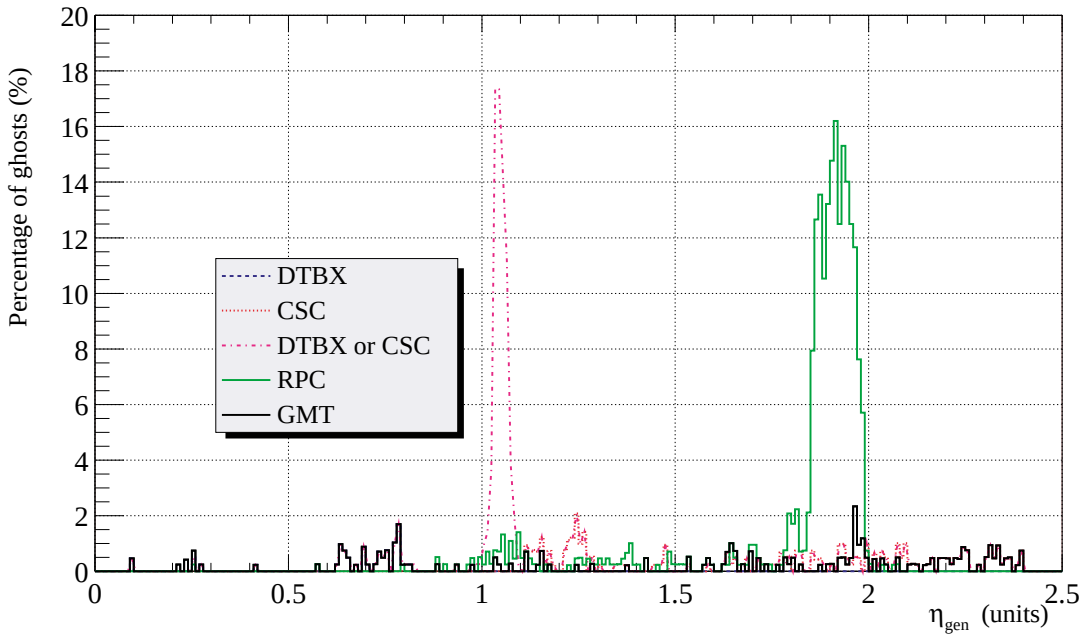

Figure 9: Percentage of ghosts (events in which one muon was generated and two or more were reported) in CSC, DT, RPC and GMT versus η. GMT fully optimized as described in Section 5. Note that ghosts in the RPC system in the region of $1.8 < |\eta| < 2.0$ are all reported with very low measured p_T (< 3.5 GeV/c) and can be removed by applying a p_T-cut.

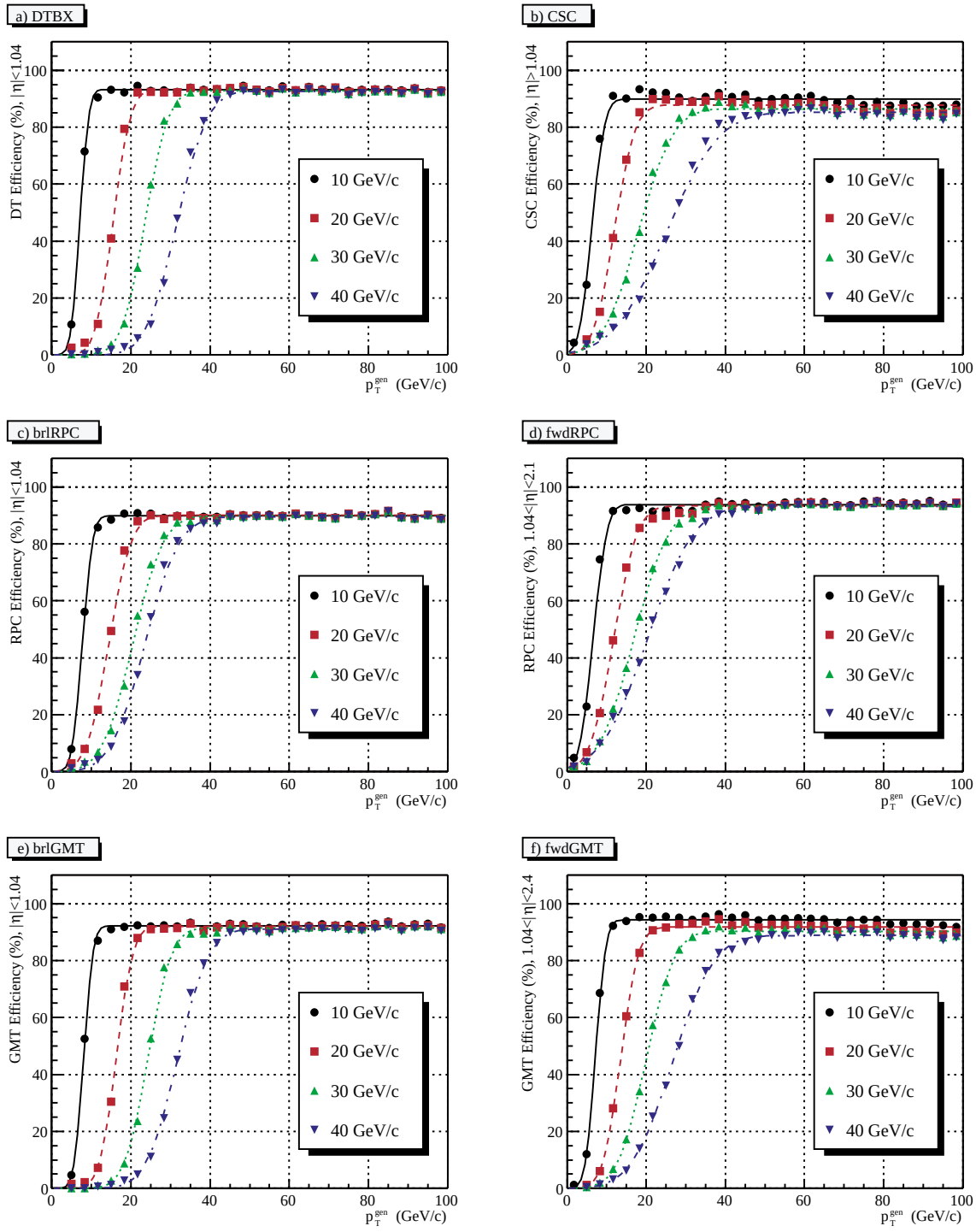

Figure 10: Turn-on curves for CSC, DT, RPC and GMT as a function of generated muon p_T for several p_T thresholds. GMT fully optimized as described in Section 5. RPC and GMT plots are shown separately for barrel and endcap.

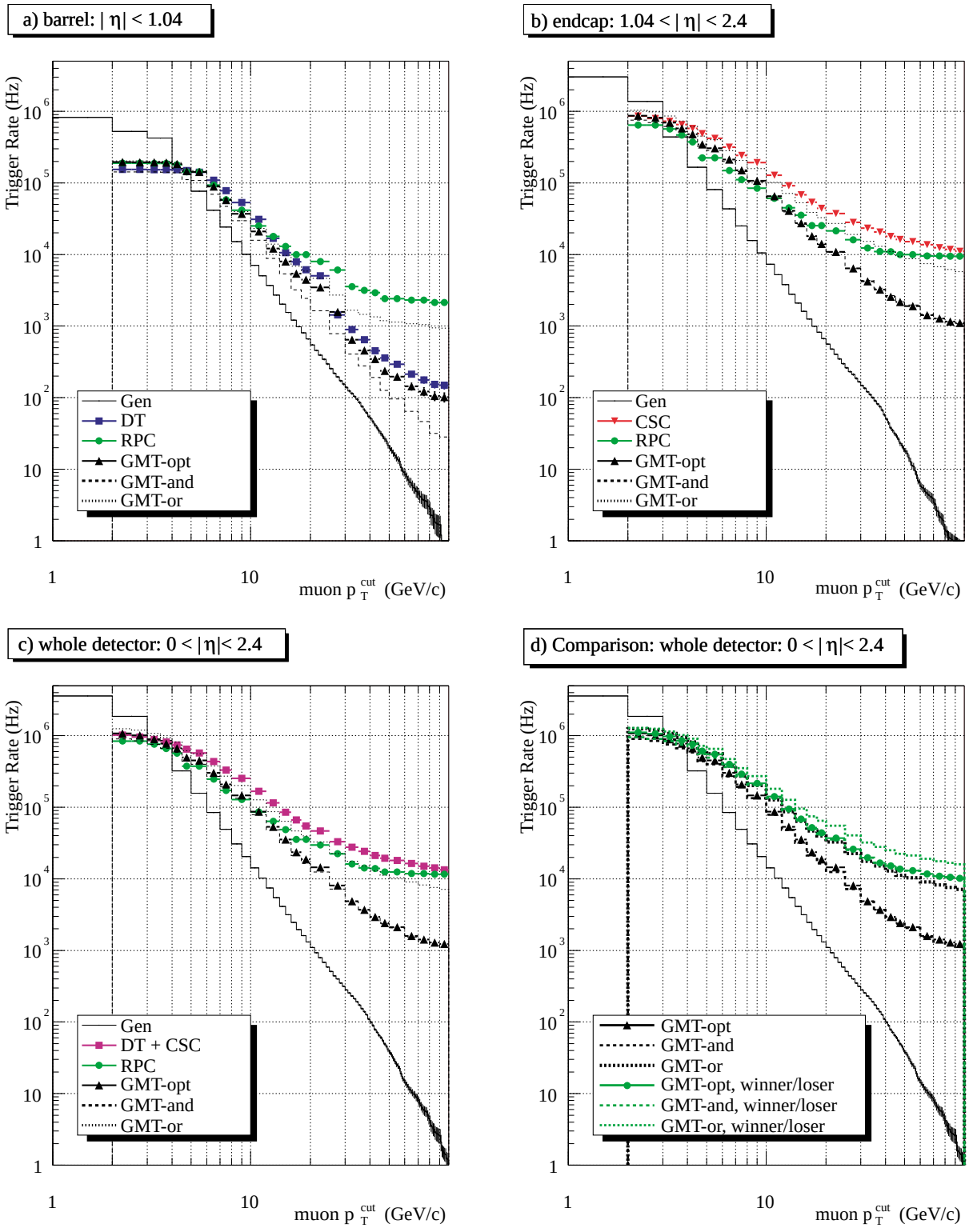

Figure 11: Integrated single muon trigger rates at L=10^{34} cm^{-2}s^{-1} for the trigger subsystems and the GMT as a function of the p_T threshold. The curves labeled "GMT-opt" show the fully optimized GMT as described in Section 5 (Muon Merger Logic in parameter mixing implementation taking the lower of the two p_T-measurements; Selection Logic optimized). Figure d) compares parameter mixing implementation and winner/loser implementation of the Muon Merger Logic as described in Subsection 5.1.

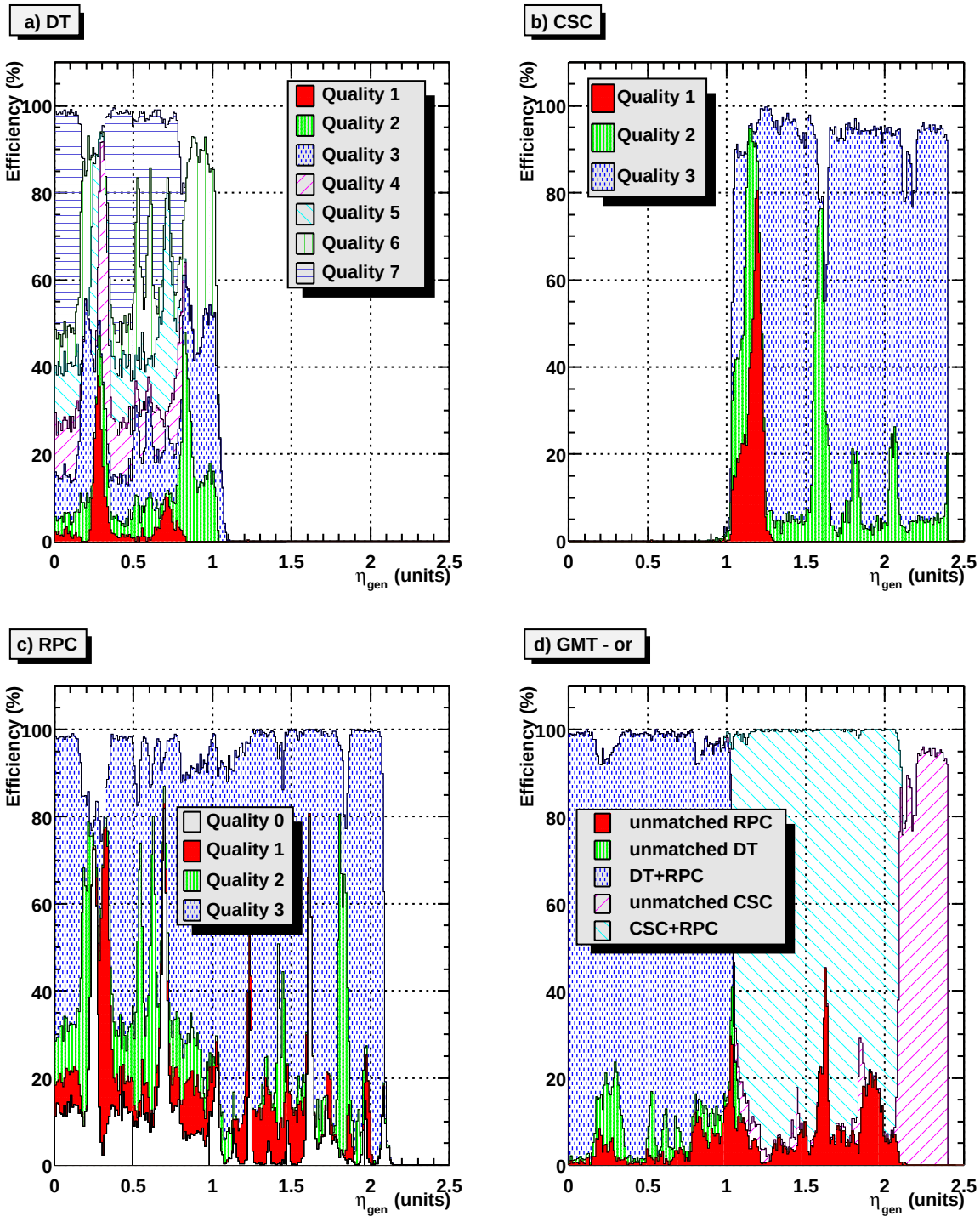

Figure 12: Efficiencies to find exactly one muon of any p_T as a function of η for different muon quality codes (see Table 1). The OR algorithm is used for the GMT Selection Logic in order to show the maximum possible GMT efficiency.

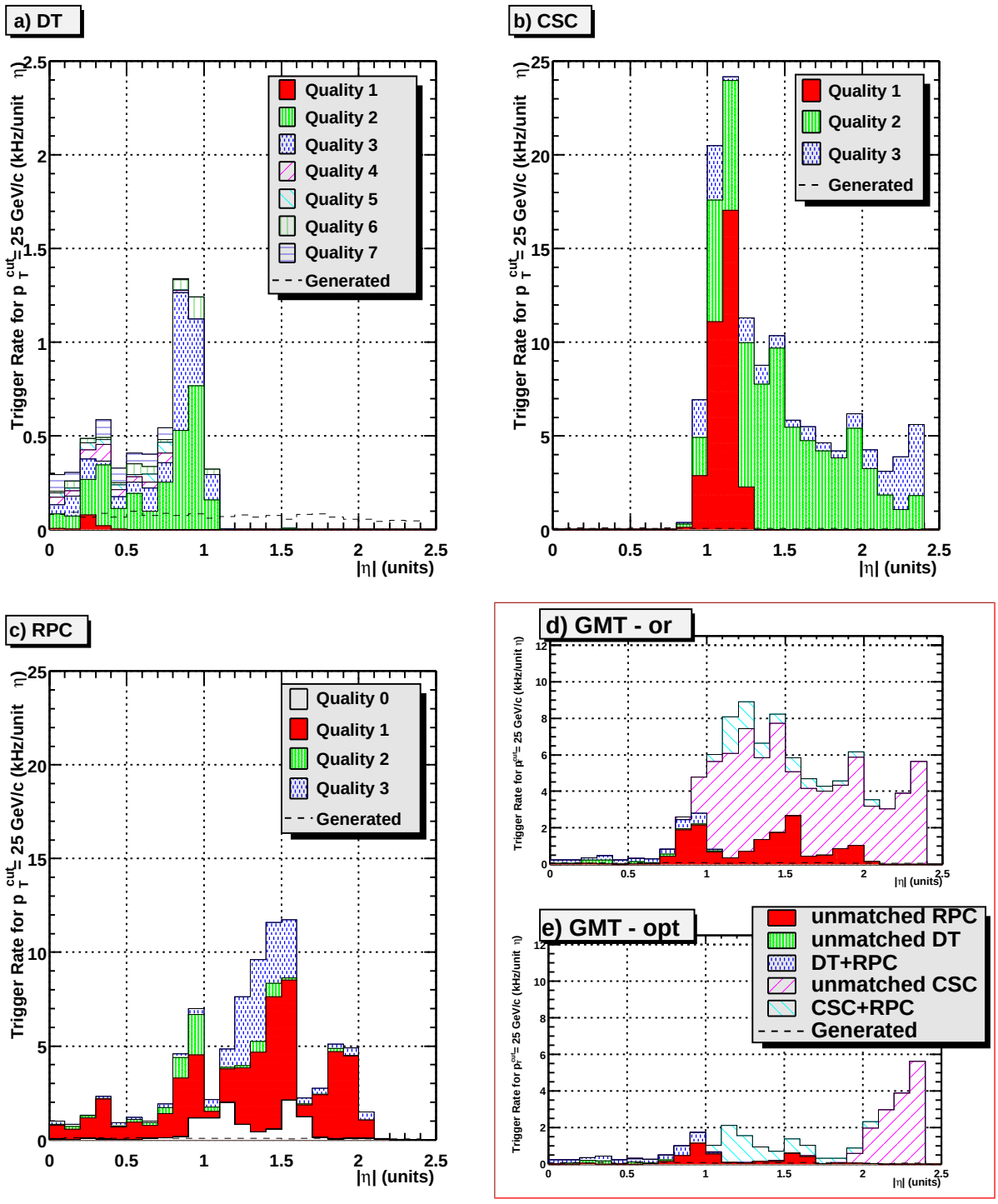

Figure 13: Integrated single muon trigger rates at L=10^{34} cm^{-2}s^{-1} for the trigger subsystems and the GMT for a p_T threshold of 25 GeV/c versus η for different muon quality codes (see Table 1). The GMT trigger rates are shown with the OR algorithm and with the optimized algorithm for the GMT Selection Logic in order to demonstrate the rate reduction achieved by optimization. Muon Merger Logic simulated in parameter mixing implementation taking lower of the two p_T measurements as described in Subsection 5.1 (default). Note that the scale for DT is 10 times smaller.

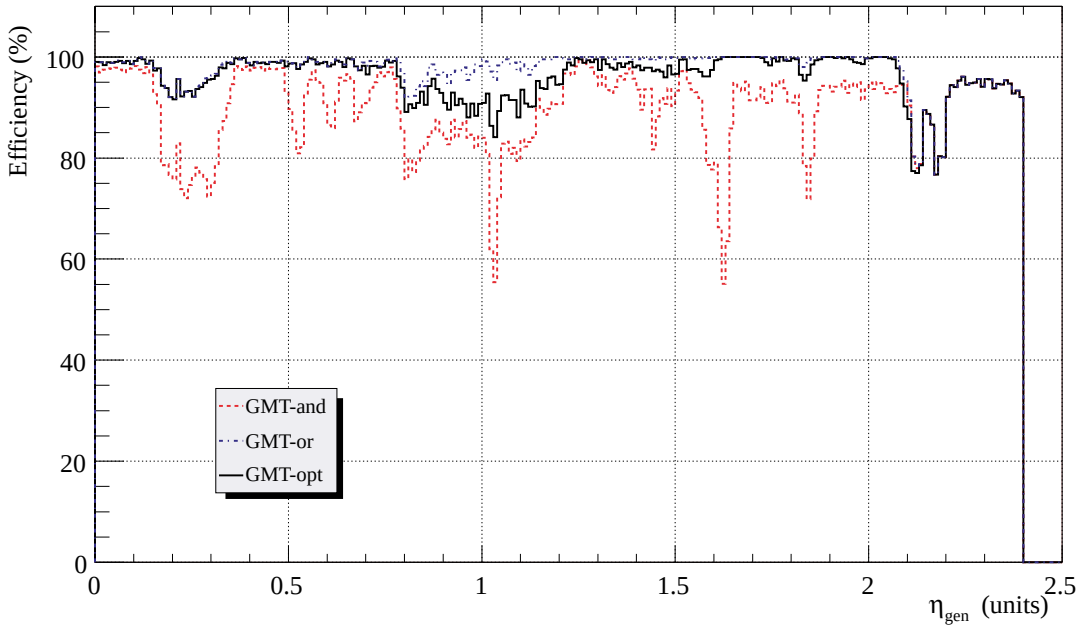

Figure 14: Efficiencies to find exactly one muon of any measured p_T as a function of generated η for three GMT selection algorithms: AND taking only muons seen by two regional triggers, OR taking all muons seen by any regional trigger and OPT optimized for efficiency, trigger rate and ghosts.

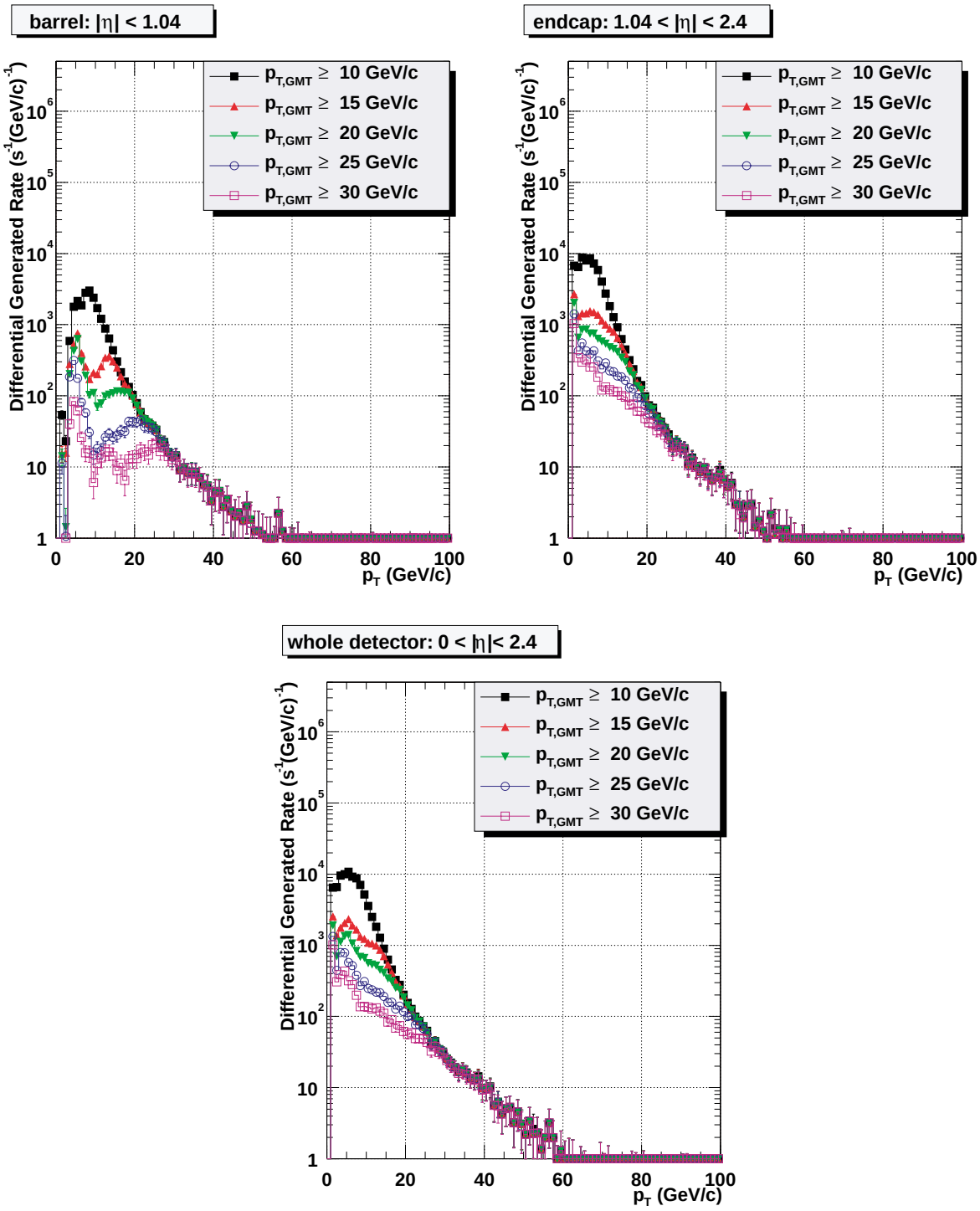

Figure 15: Differential rate of generated muons contributing to the GMT single muon trigger rate for various p_T-thresholds at L=10^{34} cm^{-2}s^{-1}. GMT fully optimized as described in Section 5 (Muon Merger Logic in parameter mixing implementation taking the lower of the two p_T-measurements; Selection Logic optimized)

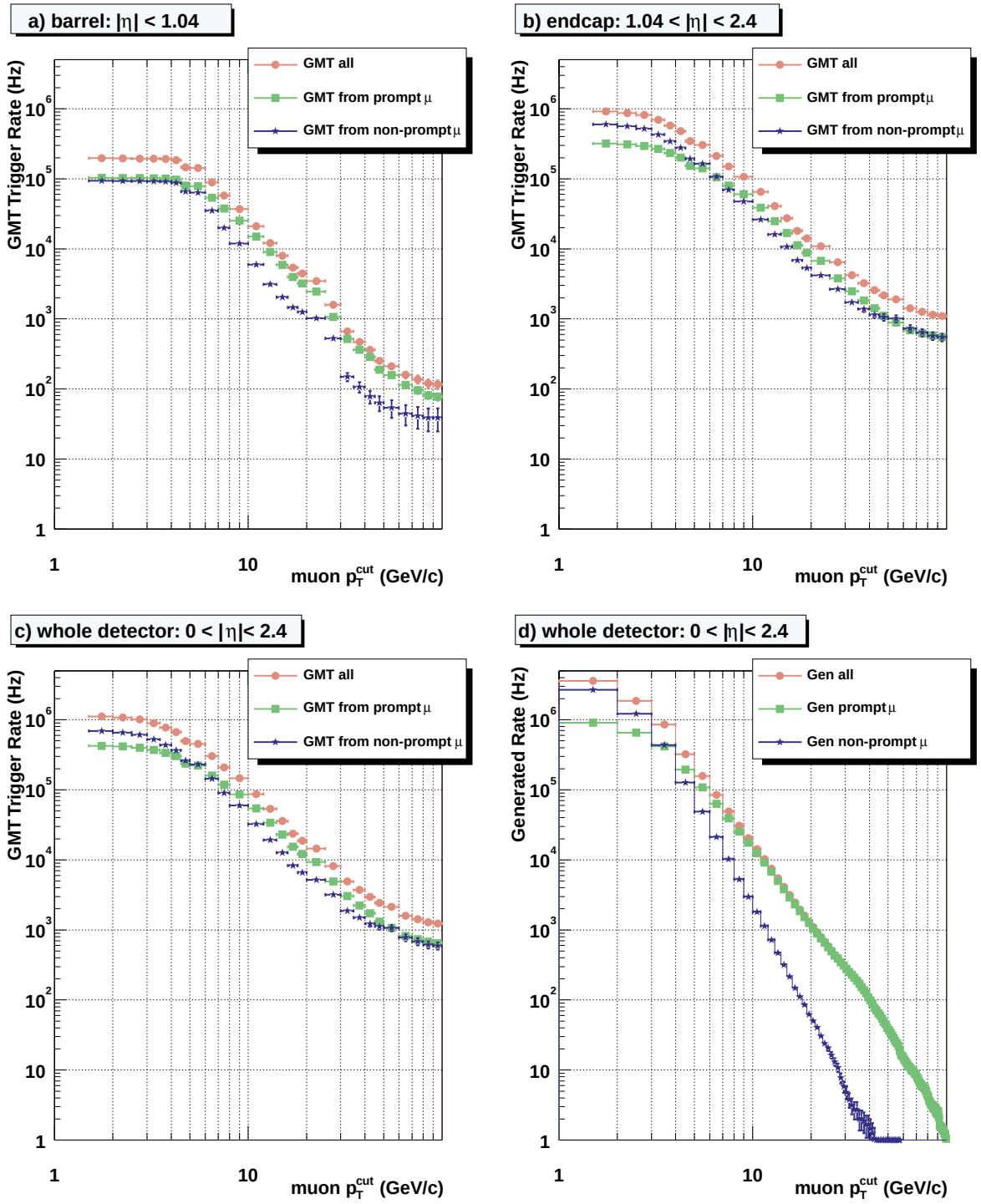

Figure 16: Integrated GMT single muon trigger rates at L=$10^{34}\,\mathrm{cm}^{-2}\mathrm{s}^{-1}$. Separate curves show trigger rates caused by prompt and non-prompt muons. GMT fully optimized as described in Section 5 (Muon Merger Logic in parameter mixing implementation taking the lower of the two p_T-measurements; Selection Logic optimized). Figure d) shows rates of generated prompt and non-prompt muons.